JACS
JOURNAL OF THE AMERICAN CHEMICAL SOCIETY
Communication
pubs.acs.org/JACS

Metal Ion Sensing Using Ion Chemical Exchange Saturation Transfer ^{19}F Magnetic Resonance Imaging

Amnon Bar-Shir,[†,‡] Assaf A. Gilad,[†,‡,§] Kannie W. Y. Chan,[†,§] Guanshu Liu,[†,§] Peter C. M. van Zijl,[†,§] Jeff W. M. Bulte,*[,†,‡,§,∥,⊥,#] and Michael T. McMahon*[,†,§]

[†]Russell H. Morgan Department of Radiology and Radiological Science, The Johns Hopkins University School of Medicine, Baltimore, Maryland 21287, United States

[‡]Cellular Imaging Section and Vascular Biology Program, Institute for Cell Engineering, The Johns Hopkins University School of Medicine, Baltimore, Maryland 21205, United States

[§]F. M. Kirby Research Center for Functional Brain Imaging, Kennedy Krieger Institute, Baltimore, Maryland 21205, United States

[∥]Department of Biomedical Engineering, The Johns Hopkins University School of Medicine, Baltimore, Maryland 21205, United States

[⊥]Department of Chemical and Biomolecular Engineering, The Johns Hopkins University, Baltimore, Maryland 21218, United States

[#]Department of Oncology, The Johns Hopkins University School of Medicine, Baltimore, Maryland 21205, United States

Supporting Information

ABSTRACT: Although metal ions are involved in a myriad of biological processes, noninvasive detection of free metal ions in deep tissue remains a formidable challenge. We present an approach for specific sensing of the presence of Ca^{2+} in which the amplification strategy of chemical exchange saturation transfer (CEST) is combined with the broad range of chemical shifts found in ^{19}F NMR spectroscopy to obtain magnetic resonance images of Ca^{2+}. We exploited the chemical shift change ($\Delta\omega$) of ^{19}F upon binding of Ca^{2+} to the 5,5′-difluoro derivative of 1,2-bis(*o*-aminophenoxy)ethane-*N*,*N*,*N*′,*N*′-tetraacetic acid (5F-BAPTA) by radiofrequency labeling at the Ca^{2+}-bound ^{19}F frequency and detection of the label transfer to the Ca^{2+}-free ^{19}F frequency. Through the substrate binding kinetics we were able to amplify the signal of Ca^{2+} onto free 5F-BAPTA and thus indirectly detect low Ca^{2+} concentrations with high sensitivity.

Metal ions play a crucial role in a myriad of biological processes, and the ability to monitor real-time changes in metal ion levels is essential for understanding a variety of physiological events. Ca^{2+} has garnered interest because of its involvement in many cellular functions and signaling pathways.[1] Currently, imaging of dynamic changes in Ca^{2+} levels is restricted to fluorescence-based methodologies,[2,3] which are limited by low tissue penetration and therefore are not suitable for in vivo Ca^{2+} imaging in deep tissues. Recent advances in the field of molecular magnetic resonance imaging (MRI) have led to the development of new strategies based on the design and synthesis of responsive contrast agents for the detection of biologically relevant metal ions. Lanthanide-based complexes[4−7] and modified superparamagnetic iron oxide[8,9] nanoparticles have been developed for Ca^{2+} sensing using MRI. 1,2-Bis(*o*-aminophenoxy)ethane-*N*,*N*,*N*′,*N*′-tetraacetic acid (BAPTA) was proposed by Tsien[10] as a Ca^{2+} indicator, and later, its 5,5′-difluoro derivative (5F-BAPTA) showed large ^{19}F NMR chemical shifts upon chelation of divalent cations.[11] The high selectivity of the binding of 5F-BAPTA to Ca^{2+} over Mg^{2+} and the high resolution of ^{19}F NMR spectra have been exploited for intracellular Ca^{2+} detection in vitro and in vivo.[11−13] However, MR spectroscopy (MRS)-based approaches rely on observation of the ^{19}F resonance of the Ca^{2+}−5F-BAPTA complex for Ca^{2+} detection, resulting in limited spatial resolution due to sensitivity considerations. One alternative, suggested by Kuchel and co-workers,[14] is the possibility of transferring magnetization between Ca^{2+}-bound and Ca^{2+}-free 5F-BAPTA during NMR experiments.

Chemical exchange saturation transfer (CEST) is a widely used MRI contrast mechanism in which a dynamic exchange process between radiofrequency (RF)-labeled protons and bulk water is exploited for contrast enhancement. CEST has been used for many applications in molecular and cellular MRI.[15−22] We employed a saturation transfer approach that couples ^{19}F and CEST MRI to sense the presence of Ca^{2+} or Mg^{2+} through their substrate binding kinetics, which we have termed ion CEST (iCEST). Using RF labeling at the ^{19}F frequency of Ca^{2+}-bound [Ca^{2+}−5F-BAPTA] and detection of the label transfer to the ^{19}F frequency of free 5F-BAPTA (0 ppm), we can amplify the signal of bound Ca^{2+} by a factor of 100. We demonstrate that the resulting *Z*-spectra display supreme sensitivity to bound Ca^{2+} over other M^{2+} cations.

Figure 1a illustrates the dynamic exchange process between free 5F-BAPTA and its complex with M^{2+}, [M^{2+}−5F-BAPTA]. Upon M^{2+} binding, there is a ^{19}F chemical shift change ($\Delta\omega$) for 5F-BAPTA. If the exchange between M^{2+}-bound and free 5F-BAPTA (with rate constant k_{ex}) is fast on the NMR time scale ($\Delta\omega \ll k_{ex}$), no peak can be resolved, as shown in Figure 1b for Mg^{2+}.

Received: April 9, 2013
Published: August 1, 2013

dx.doi.org/10.1021/ja403542g | J. Am. Chem. Soc. 2013, 135, 12164−12167

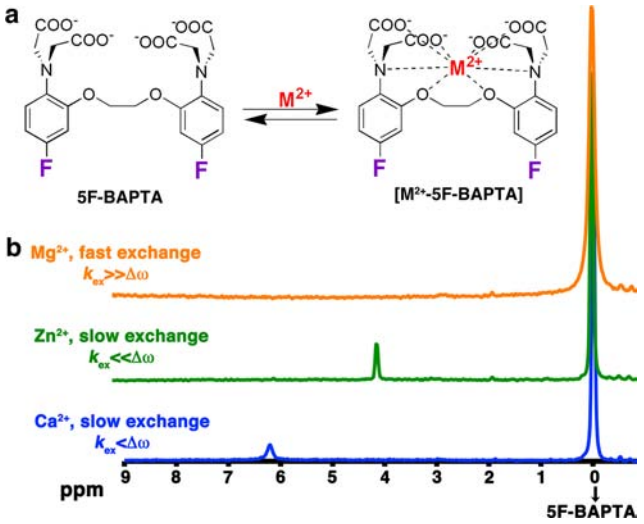

Figure 1. M^{2+} binding by 5F-BAPTA. (a) Schematic depiction of the dynamic exchange process between free 5F-BAPTA and M^{2+}-bound [M^{2+}−5F-BAPTA]. (b) ^{19}F NMR spectra (470 MHz) of 5F-BAPTA in the presence of Mg^{2+} (orange), Zn^{2+} (green), or Ca^{2+} (blue).

When the exchange is sufficiently slow at the field strength used, a well-defined peak is observed for the [M^{2+}−5F-BAPTA] resonance, as shown in Figure 1b for Zn^{2+} ($\Delta\omega \gg k_{ex}$) and Ca^{2+} ($\Delta\omega > k_{ex}$). As was previously reported, the observed $\Delta\omega$'s are typical and unique for each ion that is complexed by 5F-BAPTA and range from a few ppm in the cases of Ca^{2+}, Zn^{2+}, Ba^{2+}, Sr^{2+}, Cd^{2+}, Pb^{2+}, and others to tens of ppm upon binding of Fe^{2+}, Co^{2+}, and Ni^{2+}.[11,23] The dissociation constant (K_d) of [M^{2+}−5F-BAPTA] is different for each M^{2+} ion, and as a result, the values of k_{ex} for the process in Figure 1a also differ.[24,38] The [Zn^{2+}−5F-BAPTA] peak at 4.1 ppm (Figure 1b, green) is sharper than that of Ca^{2+}−5F-BAPTA at 6.2 ppm (Figure 1b, blue), which is correlated with their different K_d values.[23,38] Increasing the temperature from 25 to 37 °C [Figure S3 in the Supporting Information (SI)] or the addition of high concentrations of fast-exchanging ions such as K^+ and Mg^{2+} (Figure S4) leads to an upfield shift of the free 5F-BAPTA resonance in the ^{19}F NMR spectrum.

The ^{19}F iCEST properties of 5F-BAPTA in the presence of Ca^{2+} (slow-to-intermediate exchange), Zn^{2+} (very slow exchange) and Mg^{2+} (fast exchange) were determined on a 16.4 T MRI scanner at pH 7.2 (Figure 2a−c) and pH 6.4 (Figure 2d−f). A pronounced saturation transfer contrast was detected in the Ca^{2+}-containing solutions (Figure 2a,d) but not in the solutions containing Zn^{2+} (Figure 2b,e) or Mg^{2+} (Figure 2c,f). Importantly, a broad asymmetry was observed at very high fractional Mg^{2+} concentrations ($\chi_{(5F\text{-}BAPTA/Mg)}$ = 50:1; Figure S5b) that peaked at ∼1.8 ppm, a frequency much lower than for Ca^{2+} (Figure S5a). For faster ion-exchange processes between free 5F-BAPTA and M^{2+}-bound [M^{2+}−5F-BAPTA], such as that observed for Mg^{2+} (Figure S5b), other CEST imaging methods, such as frequency-labeled exchange (FLEX), may improve the detection of these ions.[36,37] Interestingly, the value of $\Delta\omega$ between [Ca^{2+}−5F-BAPTA] and free 5F-BAPTA was found to be dependent on pH (Figures 2, 3, S1, S2, and S6 and Table S1), but k_{ex} for exchange between [Ca^{2+}−5F-BAPTA] and 5F-BAPTA was preserved at all examined pH values as determined by Bloch simulations (190 ± 10 s^{-1}; Figures 2 and S1).[25]

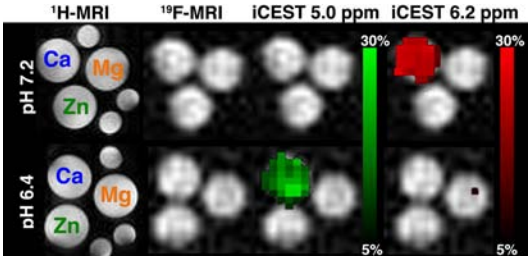

Figure 3. Imaging of Ca^{2+} with iCEST. Shown are ^{1}H MRI, ^{19}F MRI, and iCEST ($\Delta\omega$ = 6.2 or 5.0 ppm) images of M^{2+} solutions at pH 7.2 or 6.4. Each tube contained 10 mM 5F-BAPTA and 50 μM M^{2+}. Small water tubes (shown in the ^{1}H MRI images) were included to determine the orientation of the samples.

These results are in good agreement with a previous report showing that the binding of Ca^{2+} was unaffected at pH 6−8 using ^{19}F MRS.[11] ^{19}F NMR spectra collected with an internal

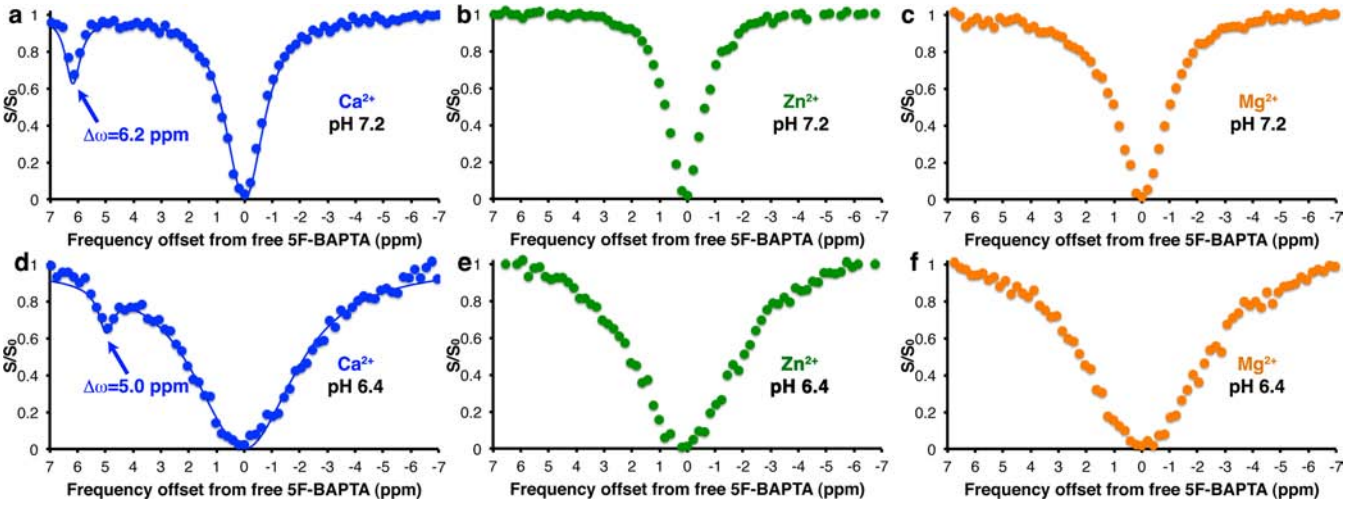

Figure 2. iCEST characteristics. Shown are ^{19}F iCEST *Z*-spectra of solutions containing 10 mM 5F-BAPTA and 50 μM Ca^{2+} (blue), Zn^{2+} (green) or Mg^{2+} (orange) in 40 mM HEPES buffer at (a−c) pH 7.2 or (d−f) pH 6.4. Dots represent the raw experimental data. For Ca^{2+}, lines represent Bloch simulations (two-pool model) and arrows point to the ^{19}F frequencies of the [Ca^{2+}−5F-BAPTA] complex.

dx.doi.org/10.1021/ja403542g | J. Am. Chem. Soc. 2013, 135, 12164−12167

reference revealed that when the pH was changed, the frequency of free 5F-BAPTA shifted but the frequency of M^{2+}-bound [M^{2+}−5F-BAPTA] did not (Figure S2). The T_2 values of 5F-BAPTA were also sensitive to pH, as can be seen by the broadening in the *Z*-spectra (Figures 2 and S1 and Table S1). The change in T_2 seemed to be dependent on 5F-BAPTA protonation rather than k_{ex}-dependent on the basis of the observation that the same line widths in the *Z*-spectra were found for solutions containing Mg^{2+} ($\Delta\omega \ll k_{ex}$) and Zn^{2+} ($\Delta\omega \gg k_{ex}$). Figure 3 shows MR images of the samples used in this study (i.e., 10 mM 5F-BAPTA with 50 μM M^{2+}). As expected, no difference in MR contrast was observed for the samples when conventional ^{1}H MRI and ^{19}F-MRI were used.

However, contrary to the Mg^{2+}- or Zn^{2+}-containing samples, which did not generate iCEST contrast at this concentration, a large iCEST contrast was detected for the Ca^{2+} containing sample when a saturation pulse (B_1 = 3.6 μT, 2000 ms) was applied at the appropriate frequency offset of the [Ca^{2+}−5F-BAPTA] complex, namely, $\Delta\omega$ = 6.2 ppm at pH 7.2 or 5.0 ppm at pH 6.4. Figure S6 shows the dependence of $\Delta\omega$ on pH, with $\Delta\omega$ ranging from 2.1 to 6.2 ppm for pH values of 5.6 to 7.2. In addition, iCEST images were acquired for solutions containing mixtures of Ca^{2+} and Mg^{2+} (50 μM Ca^{2+}, 200 μM Mg^{2+}) and Ca^{2+} and Zn^{2+} (50 μM Ca^{2+}, 50 μM Zn^{2+}) along with 10 mM 5F-BAPTA at pH 7.2. The iCEST contrast produced by Ca^{2+} was still significant (~22%) at $\Delta\omega$ = 6 ppm for all of the mixtures (Figure S5). Although high Mg^{2+} concentrations generated iCEST contrast at $\Delta\omega$ = 1.8 ppm (Figure S5a,b) the larger $\Delta\omega$ and smaller k_{ex} of [Ca^{2+}−5F-BAPTA] and its much higher iCEST contrast makes this approach better for Ca^{2+} sensing (amplification factor = 10× for Mg^{2+}, 100× for Ca^{2+}; Figure S5b).

To evaluate the sensitivity of our suggested approach, we examined the iCEST contrast at different ratios of Ca^{2+} to 5F-BAPTA (χ_{Ca}) (Figures 4a and S7). As clearly shown in Figure S7, Ca^{2+} was easily detected with iCEST MRI at χ_{Ca} = 1:1000, where ~11% contrast was observed in the *Z*-spectrum for this phantom. The same amplification was obtained when 0.5 mM 5F-BAPTA was used to detect 500 nM Ca^{2+} (Figure 4b), showing the potential of iCEST to sense low Ca^{2+} concentrations.

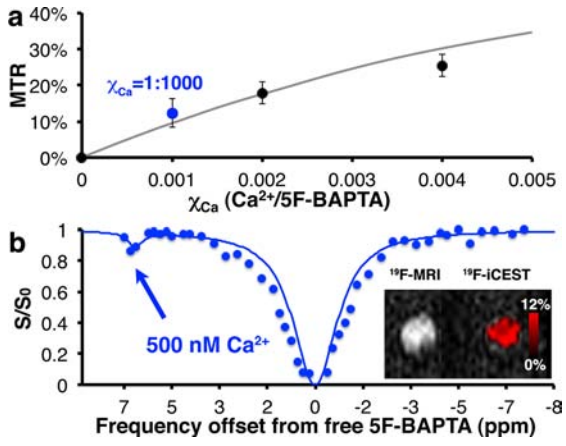

Figure 4. Ca^{2+} sensing using iCEST. (a) Plot of magnetization transfer ratio (MTR) vs χ_{Ca}. (b) Detection of 500 nM Ca^{2+} in the presence of 0.5 mM 5F-BAPTA. The inset depicts an ^{19}F MR image of the sample with an overlaid iCEST image. Lines represent Bloch simulations. Error bars represent the intervoxel standard deviations.

In this study, we have shown for the first time that spatial information on Ca^{2+} and Mg^{2+} levels can be obtained using amplification of the sensitivity by iCEST with 5F-BAPTA as the ion indicator. One advantage of using 5F-BAPTA as an MRI-responsive agent for detecting metal ions instead of probes based on ^{1}H MRI[26] or ^{129}Xe MRI[27] is that no attachment of a contrast enhancer is required. The ^{19}F atoms on the chelates serve as the responsive group as well as the contrast generator. Hyperpolarized ^{129}Xe CEST (hyperCEST)[28−30] was the first example of non-^{1}H CEST MRI, although it employs a gas bubbled into the solution instead of solute such as BAPTA. Earlier heteronuclear NMR experiments using magnetization transfer protocols have allowed the detection of exchange between two pools of nuclear spins in MRS studies.[14,31,32]

Our study shows the potential of exploiting the iCEST concept using ^{19}F MRI, as concentration ratios of 1:2000 are amplified to 1:20 changes in ^{19}F signal (Figures 4a and S7), corresponding to an amplification factor of ~100 for k_{ex} = 190 s^{-1}. In addition to the advantages of using ^{19}F MRI (i.e., high γ, 100% natural isotopic abundance, and negligible amount of ^{19}F in soft tissues),[33,34,39] the large range of ^{19}F chemical shifts (~20 times that of ^{1}H[35]) and the sensitivity of the ^{19}F $\Delta\omega$ to the details of the local environment are advantages of iCEST-based applications. One obstacle of the iCEST approach would be the detectability level of the free ^{19}F agent. This could be surmounted by collecting high-resolution ^{1}H MR images, which provide spatial information, and reducing the resolution for iCEST to allow localized detectability of the ^{19}F-based agent with improved signal-to-noise ratio (SNR)[39] (see the SI for a discussion of detectability). Using paramagnetic ^{1}H CEST probes[7] to detect Ca^{2+} should allow better spatial resolution and higher SNR than iCEST but would also have a worse sensitivity for detecting low Ca^{2+} concentrations. In the iCEST approach, the signal from the low-concentration [Ca^{2+}−5F-BAPTA] is amplified through saturation transfer onto the signal of the high-concentration free 5F-BAPTA. Since this contrast is dependent on χ_{Ca}, lower concentrations of Ca^{2+} can be detected simply by reducing the free 5F-BAPTA concentration when these concentrations are NMR-detectable.[39] This is an advantage of the iCEST approach, since this feature is not available for ^{1}H CEST, which is based on water. Finally, the unique $\Delta\omega$ found for each [M^{2+}−5F-BAPTA] and the diversity of the obtained k_{ex} values may be exploited for multi-ion MRI approaches in which each ion generates iCEST contrast with an identifiable amplitude and $\Delta\omega$. This concept was shown for different exchangeable protons in ^{1}H CEST and has been termed multicolor imaging.[17]

In conclusion, we have developed a new approach for sensing of metal ions with spatial information using MRI, in which the amplification strategy of CEST is combined with the $\Delta\omega$ specificity of the ^{19}F frequency. The outlined principles can be further extended to the design of new iCEST agents to detect other ions.

■ ASSOCIATED CONTENT

Supporting Information

Experimental methods, discussions, and simulations. This material is available free of charge via the Internet at http://pubs.acs.org.

■ AUTHOR INFORMATION

Corresponding Author

jwmbulte@mri.jhu.edu; mcmahon@mri.jhu.edu

Notes

The authors declare no competing financial interest.

■ ACKNOWLEDGMENTS

This work was supported by the Maryland Stem Cell Research Fund (MSCRFII-0161-00, MSCRFF-0103-00, MSCRFE-0040) and the NIH (R01EB012590, R01EB015031, R01EB015032).

■ REFERENCES

(1) Clapham, D. E. *Cell* **2007**, *131*, 1047.
(2) Mank, M.; Griesbeck, O. *Chem. Rev.* **2008**, *108*, 1550.
(3) Tsien, R. Y. *Annu. Rev. Neurosci.* **1989**, *12*, 227.
(4) Angelovski, G.; Fouskova, P.; Mamedov, I.; Canals, S.; Toth, E.; Logothetis, N. K. *ChemBioChem* **2008**, *9*, 1729.
(5) Dhingra, K.; Fouskova, P.; Angelovski, G.; Maier, M. E.; Logothetis, N. K.; Toth, E. *J. Biol. Inorg. Chem.* **2008**, *13*, 35.
(6) Li, W. H.; Fraser, S. E.; Meade, T. J. *J. Am. Chem. Soc.* **1999**, *121*, 1413.
(7) Angelovski, G.; Chauvin, T.; Pohmann, R.; Logothetis, N. K.; Toth, E. *Bioorg. Med. Chem.* **2011**, *19*, 1097.
(8) Atanasijevic, T.; Shusteff, M.; Fam, P.; Jasanoff, A. *Proc. Natl. Acad. Sci. U.S.A.* **2006**, *103*, 14707.
(9) Taktak, S.; Weissleder, R.; Josephson, L. *Langmuir* **2008**, *24*, 7596.
(10) Tsien, R. Y. *Biochemistry* **1980**, *19*, 2396.
(11) Smith, G. A.; Hesketh, R. T.; Metcalfe, J. C.; Feeney, J.; Morris, P. G. *Proc. Natl. Acad. Sci. U.S.A.* **1983**, *80*, 7178.
(12) Marban, E.; Kitakaze, M.; Kusuoka, H.; Porterfield, J. K.; Yue, D. T.; Chacko, V. P. *Proc. Natl. Acad. Sci. U.S.A.* **1987**, *84*, 6005.
(13) Anderson, S. A.; Song, S. K.; Ackerman, J. J.; Hotchkiss, R. S. *J. Neurochem.* **1999**, *72*, 2617.
(14) Gilboa, H.; Chapman, B. E.; Kuchel, P. W. *NMR Biomed.* **1994**, *7*, 330.
(15) Bar-Shir, A.; Liu, G.; Liang, Y.; Yadav, N. N.; McMahon, M. T.; Walczak, P.; Nimmagadda, S.; Pomper, M. G.; Tallman, K. A.; Greenberg, M. M.; van Zijl, P. C. M.; Bulte, J. W. M.; Gilad, A. A. *J. Am. Chem. Soc.* **2013**, *135*, 1617.
(16) Ratnakar, S. J.; Viswanathan, S.; Kovacs, Z.; Jindal, A. K.; Green, K. N.; Sherry, A. D. *J. Am. Chem. Soc.* **2012**, *134*, 5798.
(17) Liu, G.; Moake, M.; Har-el, Y.-e.; Long, C. M.; Chan, K. W. Y.; Cardona, A.; Jamil, M.; Walczak, P.; Gilad, A. A.; Sgouros, G.; van Zijl, P. C. M.; Bulte, J. W. M.; McMahon, M. T. *Magn. Reson. Med.* **2012**, *67*, 1106.
(18) Longo, D. L.; Busato, A.; Lanzardo, S.; Antico, F.; Aime, S. *Magn. Reson. Med.* **2012**, DOI: 10.1002/mrm.24513.
(19) Li, Y.; Sheth, V. R.; Liu, G.; Pagel, M. D. *Contrast Media Mol. Imaging* **2011**, *6*, 219.
(20) Aime, S.; Carrera, C.; Delli Castelli, D.; Geninatti Crich, S.; Terreno, E. *Angew. Chem., Int. Ed.* **2005**, *44*, 1813.
(21) Chan, K. W. Y.; Liu, G.; Song, X.; Kim, H.; Yu, T.; Arifin, D. R.; Gilad, A. A.; Hanes, J.; Walczak, P.; van Zijl, P. C. M.; Bulte, J. W. M.; McMahon, M. T. *Nat. Mater.* **2013**, *12*, 268.
(22) Liu, G.; Song, X.; Chan, K. W. Y.; McMahon, M. T. *NMR Biomed.* **2013**, *26*, 810.
(23) Kirschenlohr, H. L.; Grace, A. A.; Vandenberg, J. I.; Metcalfe, J. C.; Smith, G. A. *Biochem. J.* **2000**, *346*, 385.
(24) Csermely, P.; Sandor, P.; Radics, L.; Somogyi, J. *Biochem. Biophys. Res. Commun.* **1989**, *165*, 838.
(25) McMahon, M. T.; Gilad, A. A.; Zhou, J.; Sun, P. Z.; Bulte, J. W. M.; van Zijl, P. C. M. *Magn. Reson. Med.* **2006**, *55*, 836.
(26) Que, E. L.; Chang, C. J. *Chem. Soc. Rev.* **2010**, *39*, 51.
(27) Kotera, N.; Tassali, N.; Leonce, E.; Boutin, C.; Berthault, P.; Brotin, T.; Dutasta, J. P.; Delacour, L.; Traore, T.; Buisson, D. A.; Taran, F.; Coudert, S.; Rousseau, B. *Angew. Chem., Int. Ed.* **2012**, *51*, 4100.
(28) Schroder, L.; Lowery, T. J.; Hilty, C.; Wemmer, D. E.; Pines, A. *Science* **2006**, *314*, 446.
(29) Seward, G. K.; Bai, Y. B.; Khan, N. S.; Dmochowski, I. J. *Chem. Sci.* **2011**, *2*, 1103.
(30) Palaniappan, K. K.; Ramirez, R. M.; Bajaj, V. S.; Wemmer, D. E.; Pines, A.; Francis, M. B. *Angew. Chem., Int. Ed.* **2013**, *52*, 4849.
(31) Kupriyanov, V. V.; Balaban, R. S.; Lyulina, N. V.; Steinschneider, A.; Saks, V. A. *Biochim. Biophys. Acta* **1990**, *1020*, 290.
(32) Alger, J. R.; Shulman, R. G. *Q. Rev. Biophys.* **1984**, *17*, 83.
(33) Bulte, J. W. M. *Nat. Biotechnol.* **2005**, *23*, 945.
(34) Ruiz-Cabello, J.; Barnett, B. P.; Bottomley, P. A.; Bulte, J. W. M. *NMR Biomed.* **2011**, *24*, 114.
(35) Brey, W. S.; Brey, M. L. *Encyclopedia of Magnetic Resonance*; Wiley: Chichester, U.K., 2007; p 2063.
(36) Friedman, J. I.; McMahon, M. T.; Stivers, J. T.; Van Zijl, P. C. M. *J. Am. Chem. Soc.* **2010**, *132*, 1813.
(37) van Zijl, P. C. M.; Yadav, N. N. *Magn. Reson. Med.* **2011**, *65*, 927.
(38) Schanne, F. A.; Dowd, T. L.; Gupta, R. K.; Rosen, J. F. *Environ. Health Perspect.* **1990**, *84*, 99.
(39) Ahrens, E. T.; Zhong, J. *NMR Biomed.* **2013**, *26*, 860.